Reduced photon quenching in Ce-doped $NaYF_4$:Yb/Ho upconversion nanoparticles with core/shell structure

Shuai Ye (叶 帅), Jun Song (宋 军)*, Dong Wang (王 东), Yuliang Tian (田宇亮), Junle Qu (屈军乐), and Hanben Niu (牛憨笨)**

Key Laboratory of Optoelectronic Devices and Systems of Guangdong Province, College of Optoelectronic Engineering, Shenzhen University, Shenzhen 518060, China

**Corresponding author: songjun@szu.edu.cn; **corresponding author: jlqu@szu.edu.cn*

Received October 12, 2015; accepted December 11, 2015; posted online February 1, 2016

The use of red light or near-infrared radiation as a luminescent probe for *in vivo* bio imaging is crucial in order to restrict the strong absorption of short-wavelength light below 600 nm in tissue. It is demonstrated that the emission color of Yb/Ho codoped $NaYF_4$ nanoparticles can be tuned from green to red by incorporating Ce^{3+} ions. However, compared with that of the $NaYF_4$:Yb/Ho nanoparticles, the photoluminescence intensity of the Ce^{3+}-tridoped $NaYF_4$:Yb/Ho nanoparticles is drastically reduced. In this work, Ce^{3+}-incorporated core/shell $NaYF_4$:Yb^{3+}50%@$NaYF_4$:Ho^{3+}0.5% nanoparticles are prepared. A strong red emission and a high-intensity ratio between the red emission and green emission are obtained in these upconversion nanoparticles. The emission intensity increases by a factor higher than 120 when compared with that of the $NaYF_4$:Yb/Ho/Ce nanoparticles. This result indicates that the Ce^{3+} incorporation into the $NaYF_4$:Yb/Ho nanoparticles promotes a strong quenching effect and reduces the emission intensity; however, the quenching effect can be significantly reduced by incorporating the Ce^{3+} ions into the core/shell $NaYF_4$:Yb^{3+}50%@$NaYF_4$:Ho^{3+}0.5% nanoparticles. A theoretical model is proposed to explain the presence of the quenching effect in the $NaYF_4$:Yb/Ho/Ce nanoparticles, demonstrating that the quenching is mainly related to the interaction between the Yb^{3+} and Ce^{3+} ions.

OCIS codes: 160.2540, 160.4760.
doi: 10.3788/COL201614.021601.

Due to their interesting properties, including absence of autofluorescence, low photobleaching, strong penetration abilities, low toxicity, etc., rare-earth-doped upconversion nanoparticles (UCNPs) have attracted increasing interest[1–5]. These special features provide UCNPs with a great potential for applications in several fields, such as solar cells, solid-state lasers, boilables, and imaging[6–10]. In particular, among the various applications, *in vivo* imaging based on UCNPs is expected to be a promising photoluminescence imaging technique, as it provides high sensitivity and spatial resolution, leading to predictive models for potential clinical applications[11,12]. For *in vivo* imaging, long-wavelength light (above 600 nm) is necessary as the luminescent probe, as the tissue strongly absorbs light with a short wavelength (below 600 nm)[13]. However, three of the most important types of UCNPs, i.e., Yb/Er-, Yb/Tm-, and Yb/Ho-codoped $NaYF_4$ nanoparticles, radiate green, blue, and green light, respectively[14–18].

Presently, most of the research on red-emission UCNPs mainly focuses on the Yb/Er-codoped $NaYF_4$ nanoparticles, as they show a strong green emission (~550 nm) along with a weak dark-red emission (~660 nm). The color can be tuned from green to red using different methods: controlling the particle's size or the Yb concentration[19–22], changing the surface ligands[23,24], partially replacing the Y site of the lattice by Mn^{2+} or Zr^{4+} ions[25–30], etc. Similar to the Yb/Er-codoped $NaYF_4$ nanoparticles, the Yb/Ho-codoped $NaYF_4$ nanoparticles also show a strong green emission and a weak red emission, and it is possible to tune the emission color from green to red using different methods. Unfortunately, the tuning seems very hard to achieve. Until now, only one method has been reported to successfully tune the emission color from green to red in Yb/Ho-codoped $NaYF_4$ nanoparticles by incorporating Ce^{3+} ions and inducing a cross-relaxation process between the Ho^{3+} and Ce^{3+} ions[31–33]. However, a significant quenching effect due to the Ce incorporation was simultaneously produced, and the upconversion (UC) photoluminescence intensity of the $NaYF_4$:Yb^{3+}, Ho^{3+} 1%, Ce^{3+} 15% nanoparticles was several orders of magnitude lower than that of the $NaYF_4$:Yb^{3+}, Ho^{3+} 1% nanoparticles.

In our previous research, core/shell structured $NaYF_4$:Yb^{3+} at $NaYF_4$:Ho^{3+}1% nanoparticles were proven to enhance the red emission by increasing the Yb^{3+} concentration in the core[34]. Here, the Ce^{3+} ions were incorporated into the core/shell structured $NaYF_4$:Yb^{3+}@$NaYF_4$:Ho^{3+} nanoparticles to further enhance the red emission; in addition, a method to eliminate the quenching effect is proposed.

Two types of $NaYF_4$:Yb^{3+}50%@$NaYF_4$:Ho^{3+}0.5% nanoparticles with incorporated Ce^{3+} ions were prepared to investigate the influence of the Ce^{3+} ions. In addition, $NaYF_4$:Yb^{3+} 20%, Ho^{3+} 0.5% and $NaYF_4$:Yb^{3+} 20%, Ho^{3+} 0.5%, Ce^{3+} 20% nanoparticles were also prepared as the contrastive samples. All samples were prepared by the procedure descripted in our previous work[34]. Figure 1 shows the typical transmission electron microscopy morphologies of such nanoparticles. The monodispersed $NaYF_4$:Yb^{3+} 20%, Ho^{3+} 0.5%, Ce^{3+} 20% nanospheres exhibited an average size of ~24 nm, similar

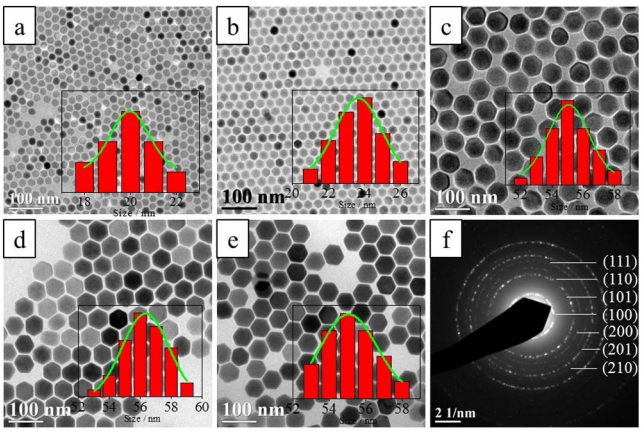

Fig. 1. Transmission electron microscopy morphologies of (a) $NaYF_4$:Yb^{3+} 20%, Ho^{3+} 1%, (b) $NaYF_4$:Yb^{3+} 20%, Ho^{3+} 0.5%, Ce^{3+} 20%, (c) $NaYF_4$:Yb^{3+}50%@$NaYF_4$:Ho^{3+}0.5%, (d) $NaYF_4$:Yb^{3+}50%@$NaYF_4$:Ho^{3+}0.5%@$NaYF_4$:Ce^{3+}20%, (e) $NaYF_4$:Yb^{3+}50%@$NaYF_4$:Ho^{3+}0.5%, Ce^{3+}20% nanoparticles (the insets show the size distribution of the corresponding nanoparticles), and (f) SAED pattern of $NaYF_4$:Yb^{3+}50%@$NaYF_4$:Ho^{3+}1%:Ce^{3+}20% nanoparticles.

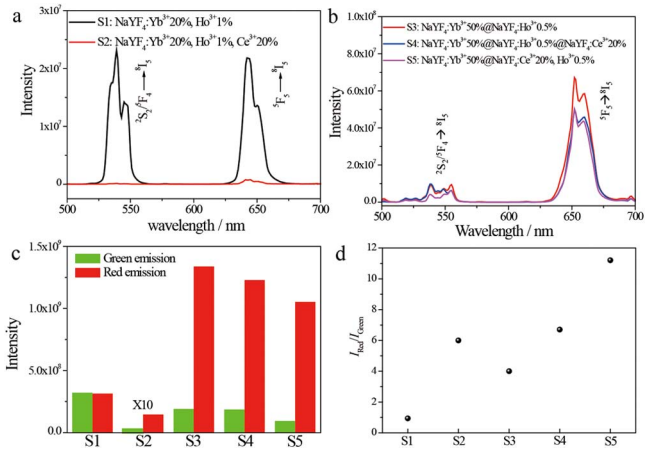

Fig. 2. Photoluminescence spectra of different types of Ce^{3+} ion incorporations: (a) $NaYF_4$:Yb^{3+} 20%, Ho^{3+} 1% and (b) $NaYF_4$:Yb^{3+}50%@$NaYF_4$:Ho^{3+}0.5% nanoparticles. (c) Photoluminescence intensity of the green and red emission bands. (d) The intensity ratios from the nanoparticles in (a) and (b).

to that of the conventional $NaYF_4$:Yb^{3+} 20%, Ho^{3+} 0.5% nanospheres, revealing that the Ce^{3+} incorporation had a minimal effect on the nanoparticle morphology and size. The $NaYF_4$:Yb^{3+}50%@$NaYF_4$:Ho^{3+}0.5% nanoparticles exhibited a hexagonal shape with an average size of ~55 nm. The larger size of these nanoparticles was mainly due to the high Yb^{3+} concentration in the core. The two types of Ce^{3+}-incorporated $NaYF_4$:Yb^{3+}50%@$NaYF_4$:Ho^{3+}0.5% nanoparticles were also hexagonal and showed a similar size to the $NaYF_4$:Yb^{3+}50%@$NaYF_4$:Ho^{3+}0.5% nanoparticles. The selected-area electron diffraction (SAED) patterns of the $NaYF_4$:Yb^{3+}50%@$NaYF_4$:Ho^{3+}0.5%, Ce^{3+}20% nanoparticles confirmed their hexagonal shape with crystallographic phases belonging to the standard hexagonal $NaYF_4$ host lattice (JCPDS 28-1192). All the results indicated that the Ce^{3+} incorporation in the $NaYF_4$:Yb^{3+}50%@$NaYF_4$:Ho^{3+}0.5% nanoparticles did not affect the microstructure, morphology, or size, as in the case of the $NaYF_4$:Yb^{3+} 20%, Ho^{3+} 1% nanoparticles.

The photoluminescence spectra of the nanoparticles, with and without incorporated Ce^{3+}, were measured using a 980 nm laser excitation, as shown in Fig. 2. The photoluminescence intensity of $NaYF_4$:Yb^{3+} 20%, Ho^{3+} 1%, Ce^{3+} 20% was reduced by 97%, although the I_{Red}/I_{Green} ratio was enhanced from 0.9 to 7 compared with that of the $NaYF_4$:Yb^{3+} 20%, Ho^{3+} 1% nanoparticles (Fig. 2(a)). This result revealed a strong quenching effect in the nanoparticles due to the Ce^{3+} incorporation. However, a slight effect of the Ce^{3+} incorporation on the emission intensity was observed in the $NaYF_4$:Yb^{3+}50%@$NaYF_4$:Ho^{3+} 0.5% nanoparticles, as shown in Fig. 2(b). Compared with the $NaYF_4$:Yb^{3+}50%@$NaYF_4$:Ho^{3+}0.5% nanoparticles without incorporated Ce^{3+}, the photoluminescence intensity of the $NaYF_4$:Yb^{3+}50%@$NaYF_4$:Ho^{3+}0.5% nanoparticles shelled by $NaYF_4$:Ce^{3+} 20% was reduced by ~8%, and the I_{Red}/I_{Green} ratio was approximately equal to 7, slightly higher than that of the $NaYF_4$:Yb^{3+}50%@$NaYF_4$:Ho^{3+}0.5% nanoparticles. This result indicated that an enhancement of the red emission of the $NaYF_4$:Yb^{3+}50%@$NaYF_4$:Ho^{3+}0.5% nanoparticles was not achievable by only coating them with a Ce^{3+}-contained shell layer. When the Ce^{3+} ions were incorporated into the shell of the $NaYF_4$:Yb^{3+}50%@$NaYF_4$:Ho^{3+}0.5%, Ce^{3+}20% nanoparticles, the I_{Red}/I_{Green} ratio was enhanced to 11, nearly twice that of the $NaYF_4$:Yb^{3+}50%@$NaYF_4$:Ho^{3+}0.5% nanoparticles, although the photoluminescence intensity was also reduced by ~22%. However, the emission intensity of the $NaYF_4$:Yb^{3+}50%@$NaYF_4$:Ho^{3+}0.5%, Ce^{3+}20% nanoparticles was enhanced by a factor of more than 120 compared with that of the $NaYF_4$:Yb^{3+} 50%, Ho^{3+} 1%, Ce^{3+} 20% nanoparticles. These results demonstrated the weak quenching effect that exists in the $NaYF_4$:Yb^{3+}50%@$NaYF_4$:Ho^{3+}0.5%, Ce^{3+}20% nanoparticles.

The dependence of the intensities of the green and the red UC emission band on the pump power for the $NaYF_4$:Yb^{3+}50%@$NaYF_4$:Ho^{3+}0.5%, Ce^{3+}20% UCNPs was measured, as shown in Fig. 3. In general, the photoluminescence intensity increased on the pump laser power and obeyed the rule of $I_{UCL} \propto p^n$, where I_{UCL} is the photoluminescence intensity, p is the pump laser power, and n is the number of laser photons required. The slope values for the green and the red emission bands of the $NaYF_4$:Yb^{3+}50%@$NaYF_4$:Ho^{3+}0.5%, Ce^{3+}20% UCNPs approached 2, indicating that both the green and the red emissions involve a two-photon process for their generations. The slope values were in good agreement with previous results on Yb^{3+}/Ho^{3+}-codoped UCNPs[32,34].

High emission intensity was observed in the core/shell nanoparticles consisting of a core containing Yb^{3+} ions and a shell containing Ho^{3+} and Ce^{3+} ions. This result

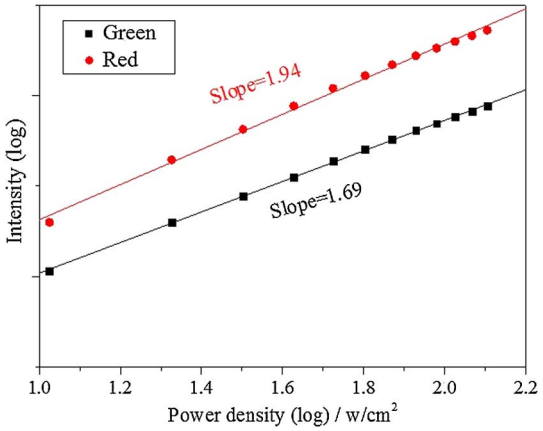

Fig. 3. Logarithmic plot of the dependence of the intensities of the green and the red UC emission bands on the pump power for the $NaYF_4$:Yb^{3+}50%@$NaYF_4$:Ho^{3+}1%, Ce^{3+}20% UCNPs.

implied that the strong quenching effect in the Yb/Ho/Ce-tridoped $NaYF_4$ nanoparticles may be related to the interaction between the Yb^{3+} and Ce^{3+} ions. To verify and provide a theoretical background to this hypothesis, the steady-state rate equations were used. In this physical model, N_{Yb0} and N_{Yb1} are the population densities of the Yb^{3+} ions in the ground and the excited states, respectively; N_0, N_1, N_2, N_3, and N_4 are the population densities of the $^5I_8$, $^5I_7$, $^5I_6$, $^5F_5$, and $^5S_2/^5F_4$ states, respectively, of the Ho^{3+} ions; and N_{Ce0} and N_{Ce1} are the population densities of the Ce^{3+} ions in the ground and the excited states, respectively. In addition, W_0, W_1, and W_2 are the energy transfer rates from the excited Yb^{3+} ions to the Ho^{3+} ions, and R_1, R_2, R_3, and R_4 are the radiation rates of the energy states of the Ho^{3+} ions. β_1 and β_2 are the phonon-assisted nonradiative relaxation rates from the $^5I_6$ to $^5I_7$ and from the $^5S_2/^5F_4$ to $^5F_5$ states, respectively, of the Ho^{3+} ions; C_2 and C_4 are the coefficients of the cross relaxations between Ho^{3+} and Ce^{3+} ions in the $^5I_6$ and $^5S_2/^5F_4$ states, respectively; and M is the coefficient of the cross relaxation between the Yb^{3+} and Ce^{3+} ions. I is the laser intensity at 980 nm, ν is the laser frequency, σ_{Yb} is the absorption cross section of the Yb^{3+} ion, R is the radiation rate of the excited state of Yb^{3+}, and R_{Ce} is the radiation rate of the excited state of Ce^{3+}. The steady-state rate equations for the discussed system can be described as follows:

$$0=\frac{dN_1}{dt}=\beta_1 N_2+C_2N_2N_{Ce0}-R_1N_1-W_1N_{Yb1}N_1, \quad (1\text{-}1)$$

$$0=\frac{dN_2}{dt}=W_0N_{Yb1}N_0-\beta_1N_2-C_2N_2N_{Ce0}-R_2N_2-W_2N_{Yb1}N_2, \quad (1\text{-}2)$$

$$0=\frac{dN_3}{dt}=W_1N_{Yb1}N_1+C_4N_4N_{Ce0}-R_3N_3+\beta_2N_4, \quad (1\text{-}3)$$

$$0=\frac{dN_4}{dt}=W_2N_{Yb1}N_2-R_4N_4-C_4N_4N_{Ce0}-\beta_2N_4, \quad (1\text{-}4)$$

$$0=\frac{dN_{Yb1}}{dt}=\frac{I}{h\nu}\sigma_{Yb}N_{Yb}-R_{Yb}N_{Yb1}-(W_0N_0+W_1N_1+W_2N_2)N_{Yb1}-MN_{Ce0}N_{Yb1}, \quad (2\text{-}1)$$

$$0=\frac{dN_{Ce1}}{dt}=C_2N_2N_{Ce0}+C_4N_4N_{Ce0}+MN_{Ce0}N_{Yb1}-R_{Ce}N_{Ce1}. \quad (2\text{-}2)$$

After solving Eqs. (1) and (2), we obtained the following expressions:

$$N_1=\left[\frac{(\beta_1+C_2N_{Ce0})W_0N_0}{R_1(\beta_1+C_2N_{Ce0}+R_2)}-\frac{W_1}{R_1}\right]N_{Yb1}, \quad (3)$$

$$N_2=\frac{W_0N_0}{\beta_1+C_2N_{Ce0}+R_2+W_2N_{Yb1}}N_{Yb1}, \quad (4)$$

$$N_3=\left[\frac{(\beta_1+C_2N_{Ce0})W_1}{R_1+W_1N_{Yb1}}+\frac{(\beta_2+C_4N_{Ce0})W_2}{R_4+C_4N_{Ce0}+\beta_2}\right]\times\frac{W_0N_0(N_{Yb1})^2}{(R_2+\beta_1+C_2N_{Ce0}+W_2N_{Yb1})R_3}, \quad (5)$$

$$N_4=\frac{W_0W_2N_0(N_{Yb1})^2}{(R_4+C_4N_{Ce0}+\beta_2)(R_2+C_2N_{Ce0}+\beta_1+W_2N_{Yb1})}, \quad (6)$$

$$N_{Yb1}=\frac{I\sigma_{Yb}N_{Yb0}}{h\nu(R_{Yb}+W_0N_0+W_1N_1+W_2N_2+MN_{Ce0})}, \quad (7)$$

$$N_{Ce0}=\frac{R_{Ce}N_{Ce1}}{C_2N_2+C_4N_4+MN_{Yb1}}. \quad (8)$$

Then, we can obtain the intensities of the red and green lights by applying the following equations:

$$I_r=N_3h\nu_rR_3, \quad (9)$$

$$I_g=N_4h\nu_gR_4, \quad (10)$$

where ν_r and ν_g are the frequencies of the red light and green light, respectively. Furthermore, by combining Eqs. (5), (6), (9), and (10), we can derive the following expressions:

$$I_r=\left[\frac{(\beta_1+C_2N_{Ce0})W_1}{R_1+W_1N_{Yb1}}+\frac{(\beta_2+C_4N_{Ce0})W_2}{R_4+C_4N_{Ce0}+\beta_2}\right]\times\frac{W_0N_0(N_{Yb1})^2}{(R_2+\beta_1+C_2N_{Ce0}+W_2N_{Yb1})}h\nu_r, \quad (11)$$

$$I_g=\frac{R_4W_0W_2N_0(N_{Yb1})^2}{(R_4+C_4N_{Ce0}+\beta_2)(R_2+C_2N_{Ce0}+\beta_1+W_2N_{Yb1})}h\nu_g. \quad (12)$$

According to Eqs. (7) and (8), we know that

$$N_{\mathrm{Yb1}}, N_{\mathrm{Ce0}} \propto \frac{1}{1+M}. \tag{13}$$

Moreover, considering Eqs. (11) and (12), we can also obtain the following expressions:

$$I_r \propto \frac{1}{(1+M)^2[R_2+\beta_1+C_2(1+M)+W_2(1+M)]}, \tag{14}$$

$$I_g \propto \frac{1}{[(R_4+\beta_2)(1+M)+C_4][(R_2+\beta_1)(1+M)+C_2+W_2]}. \tag{15}$$

Hence, from Eqs. (14) and (15), it was demonstrated that both the intensities of the red and green lights decrease by the coefficient M of the cross relaxation between Yb^{3+} and Ce^{3+} ions, although the two cross relaxations between Ho^{3+} and Ce^{3+} ions can lead to an enhancement of the red light radiation by reducing the green light radiation, as shown in Fig. 4(b). This model is able to explain the low emission intensity of the Yb/Ho/Ce-tridoped $NaYF_4$ nanoparticles. When the Ho^{3+} and Ce^{3+} ions were moved to the shell layer, as shown in Fig. 4(c), the cross relaxation between the Yb^{3+} and Ce^{3+} ions could be reduced drastically as a result of the extended distance between the Yb^{3+} and Ce^{3+} ions, while the cross relaxation between the Ho^{3+} and Ce^{3+} ions was kept constant. Thus, high-intensity red light radiation was obtained for the $NaYF_4$:Yb^{3+}50%@$NaYF_4$:Ho^{3+}0.5%, Ce^{3+}20% nanoparticles. The ~22% reduction of the $NaYF_4$:Yb^{3+}50%@$NaYF_4$:Ho^{3+}0.5%, Ce^{3+}20% nanoparticles, compared with that of the $NaYF_4$:Yb^{3+}50%@$NaYF_4$:Ho^{3+}0.5% nanoparticles (Fig. 2), mainly resulted from the cross relaxation between the Yb^{3+} and Ce^{3+} ions at the core/shell interface. The ~8% reduction of the $NaYF_4$:Yb^{3+}50%@$NaYF_4$:Ho^{3+}0.5%@$NaYF_4$:Ce^{3+}20% nanoparticles indicated that the quenching effect was further reduced by extending the distance between the Yb^{3+} and Ce^{3+} ions.

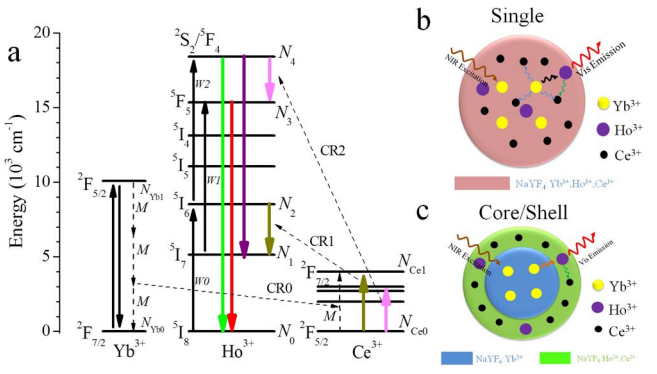

Fig. 4. (a) Energy level diagrams of Ho^{3+}, Yb^{3+}, and Ce^{3+} ions and proposed UC mechanisms. (b) Schematic illustration of the proposed energy-transfer mechanisms in $NaYF_4$:Yb/Ho/Ce nanoparticles. (c) Schematic illustration of the proposed energy-transfer mechanisms in core/shell $NaYF_4$:Yb@$NaYF_4$:Ho/Ce nanoparticles.

In conclusion, the Ce^{3+} ions are incorporated into the Yb/Ho-codoped $NaYF_4$ nanoparticles to enhance the red emission. The Ce^{3+} incorporation enhances the intensity ratio between the red emission and the green emission of the $NaYF_4$:Yb/Ho nanoparticles, but largely reduces the total photoluminescence intensity. However, when the Ce^{3+} ions are incorporated into the shell of the core/shell $NaYF_4$:Yb^{3+}50%@$NaYF_4$:Ho^{3+}0.5% nanoparticles, the emission intensity is also enhanced by a factor of more than 120 compared with that of the $NaYF_4$:Yb/Ho/Ce nanoparticles. This result indicates that the Ce^{3+} incorporation into the $NaYF_4$; Yb/Ho nanoparticles promotes a strong quenching effect that reduces the emission intensity; the quenching effect is significantly reduced by incorporating the Ce^{3+} ions into the core/shell structured Yb/Ho codoped $NaYF_4$ nanoparticles. A theoretical model is proposed to explain the quenching effect existing in the $NaYF_4$:Yb/Ho/Ce nanoparticles, revealing that the quenching is mainly related to the interaction between the Yb^{3+} ions and the Ce^{3+} ions.

This work was partially supported by the National Basic Research Program of China (Nos. 2015CB352005 and 2012CB825802), the National Natural Science Foundation of China (Nos. 61378091 and 61405123), and the Shenzhen science and Technology Project (No. JCYJ20150324141715561).

References

1. S. Gai, C. Li, P. Yang, and J. Lin, Chem. Rev. **114**, 2343 (2014).
2. F. Huang, X. Liu, W. Li, L. Hu, and D. Chen, Chin. Opt. Lett. **12**, 051601 (2014).
3. J. Shen, L. Zhao, and G. Han, Adv. Drug Delivery Rev. **65**, 744 (2013).
4. G. Chen, H. Ågren, T. Ohulchanskyya, and P. N. Prasad, Chem. Soc. Rev. **44**, 1680 (2015).
5. X. Yu, L. Chen, M. Li, M. Xie, L. Zhou, Y. Li, and Q. Wang, Adv. Mater. **20**, 4118 (2008).
6. G. Chen, J. Seo, C. Yang, and P. N. Prasad, Chem. Soc. Rev. **42**, 8304 (2013).
7. L. Zhou, Z. Li, Z. Liu, M. Yin, J. Ren, and X. Qu, Nanoscale **6**, 1445 (2014).
8. R. Lei, H. Wang, S. Xu, Y. Tian, and L. Huang, Chin. Opt. Lett. **2**, 021602 (2015).
9. G. Chen, T. Y. Ohulchanskyy, S. Liu, W. C. Law, F. Wu, M. T. Swihart, H. Agren, and P. N. Prasad, ACS Nano **6**, 2969 (2012).
10. J. Liu, W. Bu, L. Pan, and J. Shi, Angew. Chem. Int. Ed. **52**, 4375 (2013).
11. Y. Zhou, S. T. Han, X. Chen, F. Wang, Y. B. Tang, and V. Roy, Nat. Commun. **4**, 1 (2014).
12. K. Koenig, J. Microscopy **200**, 83 (2000).
13. A. Xia, M. Chen, Y. Gao, D. Wu, W. Feng, and F. Li, Biomaterials **33**, 5394 (2012).
14. J. Boyer, F. Vetrone, L. A. Cuccia, and J. A. Capobianco, J. Am. Chen. Soc. **128**, 7444 (2006).
15. S. Heer, K. Kompe, H. U. Gudel, and M. Haase, Adv. Mater. **16**, 2102 (2004).

16. H. Mai, Y. Zhang, L. Sun, and C. Yan, J. Phys. Chem. C **111**, 13721 (2007).
17. Y. Zhao, Q. Zhan, J. Liu, and S. He, Biomed. Opt. Express **6**, 838 (2015).
18. J. Liu, R. Wu, N. Li, X. Zhang, and Q. Zhan, Biomed. Opt. Express **6**, 1857 (2015).
19. A. Punjabi, X. Wu, A. Tokatli-Apollon, M. El-Rifai, H. Lee, Y. Zhang, C. Wang, Z. Liu, E. M. Chan, C. Duan, and G. Han, ACS Nano **8**, 10621 (2014).
20. J. Shen, G. Chen, T. Y. Ohulchanskyy, S. J. Kesseli, S. Buchholz, Z. Li, P. N. Prasad, and G. Han, Small **9**, 3212 (2013).
21. W. Wei, Y. Zhang, R. Chen, J. Goggi, N. Ren, L. Huang, K. K. Bhakoo, H. Sun, and T. T. Yang Tan, Chem. Mater. **26**, 5183 (2014).
22. H. Qian and Y. Zhang, Langmuir **24**, 12123 (2008).
23. W. Niu, S. Wu, and S. Zhang, J. Mater. Chem. **21**, 10894 (2011).
24. W. Niu, S. Wu, and S. Zhang, J. Mater. Chem. **20**, 9113 (2010).
25. Q. Dou, N. M. Idris, and Y. Zhang, Biomaterials **34**, 1722 (2013).
26. F. Wang and X. Liu, J. Am. Chem. Soc. **130**, 5642 (2008).
27. G. Tian, Z. Gu, L. Zhou, W. Yin, X. Liu, L. Yan, S. Jin, W. Ren, G. Xing, S. Li, and Y. Zhao, Adv. Mater. **24**, 1226 (2012).
28. H. Wang, W. Lu, Z. Yi, L. Rao, S. Zeng, and Z. Li, J. Alloys Comp. **618**, 776 (2015).
29. J. Wang, F. Wang, C. Wang, Z. Liu, and X. Liu, Angew. Chem. Int. Ed. **50**, 10369 (2011).
30. D. Chen, L. Lei, R. Zhang, A. Yang, J. Xu, and Y. Wang, Chem. Commun. **48**, 10630 (2012).
31. W. Gao, H. Zheng, Q. Han, E. He, F. Gao, and R. Wang, J. Mater. Chem. C **2**, 5327 (2014).
32. G. Chen, H. Liu, G. Somesfalean, H. Liang, and Z. Zhang, Nanotechnology **20**, 385704 (2009).
33. D. Chen, Y. Zhou, Z. Wan, Z. Ji, and P. Huang, Dalton Trans. **44**, 5288 (2015).
34. S. Ye, G. Chen, W. Shao, J. Qu, and P. N. Prasad, Nanoscale **7**, 3976 (2015).